Enhancement of the structural, morphological, optical, and electrical properties of Mn doped CuO thin films via spray pyrolysis

P. DATTA[1,2], M. SHARMIN[3], J. PODDER[3,*], S. CHOUDHURY[1]
[1]Department of Physics, University of Dhaka, Dhaka-1000, Bangladesh
[2]Nuclear Power Plant Company Bangladesh Limited, Rooppur NPP Bhaban, Dhaka-1000, Bangladesh
[3]Department of Physics, Bangladesh University of Engineering and Technology, Dhaka-1000, Bangladesh

Manganese (Mn) doped copper (II) oxide (CuO) thin films with 0 to 6 at% Mn doping were prepared onto the glass substrates at a temperature of 523 K using spray pyrolysis technique. The CuO and Mn doped CuO films showed monoclinic structure with the preferential orientation along ($\bar{1}$11) and (111) planes after being annealed at 723 K in air for 60 min. The film surface was observed to be comprised of agglomerated nanoparticles under Scanning Electron Microscopy. Elemental composition of the films was confirmed by Energy Dispersive X-ray analysis. Optical transmittance and band gap of CuO thin film increased with Mn doping up to 4 at% in the visible-infrared region of light. Electrical resistivity of the samples decreased from 2.69×10^3 to 1.62×10^3 Ω-m with the increase of Mn doping. Activation energy of the films varied from 0.08 to 0.29 eV in the temperature region 323 - 383 K, whereas it varied from 0.29 to 0.40 eV in the temperature region 383 - 423 K.

1. Introduction

Copper (II) oxide (CuO) is an important p-type transition metal oxide which has drawn the attention of researchers because of its availability in nature, low-cost, non-toxic and relatively simple formation of oxide nanostructures [1, 2]. Undoped and doped CuO thin films have been studied for several potential applications such as solar cells, transistors, gas sensors, etc. [3-7]. Substantial changes in structure and properties of CuO were found after doping transition metals like zinc (Zn) [8], manganese (Mn) [9], cobalt (Co) [10], cadmium (Cd) [11], etc. Mn is one of the popular dopants for CuO because of the nearly equal cationic radii of Mn^{2+} (83 pm) and Cu^{2+} (73 pm) [12]. These comparable ionic radii can be beneficial for creation of Cu^{2+} substitutions via Mn^{2+} in the CuO lattice and cause significant improvement in the morphological properties of CuO. It is expected that incorporation of Mn^{2+} will create impurity energy states within the band gap which will be used as interim steps for electrons during valence-conduction band transition [13]. As a consequence, changes in optical and electrical properties of CuO are predicted to occur via Mn doping. Mn doped CuO thin films were deposited via several techniques such as electrodeposition [14], radio frequency magnetron sputtering [15], plasma enhanced chemical vapor deposition [16], sol-gel [17], spray pyrolysis [18], etc. Each deposition technique has its own advantages and disadvantages. Among the techniques, spray pyrolysis is a simple and popular one because of its advantages of large area deposition of dense and porous films, good microstructural and compositional control, no requirement of vacuum, versatility of choice of precursor,

etc. [19]. In an earlier literature, the optimized substrate temperature was found to be 523 K for deposition of CuO thin film [20]. Sometimes, the as-deposited thin films are annealed for betterment of their structure, morphology and properties [21]. Mn doped CuO thin films were prepared from 0, 2 and 4 % volumetric ratios of $CuCl_2.2H_2O$ and $MnCl_2.4H_2O$ precursors using spray pyrolysis technique [18]. The samples were prepared at 300 °C substrate temperature followed by an annealing process at the temperature of 400 °C for 3 hours. They reported that 2 % Mn doped film had smaller crystallite size and smoother surface compared to others, in contrast higher Mn concentration showed higher antibacterial activity against *E. coli* and *S. aureus* bacteria. Hussin et al. [22] prepared Mn doped CuO thin films with 2 and 4 % Mn doping by spray pyrolysis of aqueous solution of cupric chloride and manganese chloride precursors at 450 °C substrate temperature and using N_2 as the transporter gas. They found polycrystalline monoclinic structure of the deposited films with the preferred orientation along (002) plane, smooth surface morphology and optical band gap ranging from 1.72 to 1.92 eV. Ismail et al. [23] synthesized 0, 3, 5, 7 and 9 wt% Mn doped CuO thin films by spray pyrolysis of chloride precursors at 400 °C substrate temperature. They reported the decrease of grain size and surface roughness with the increase of Mn doping in CuO thin films. Babu and Podder [24] carried out theoretical first principles-based density functional theory calculations and experimental work on 0, 2, 4, 6 and 8 at% Mn doped CuO thin films prepared at 325 °C using thermal spray pyrolysis. They reported the higher Cu-O bond length and reversal of electrical conductivity from p to n-type for 4 at% Mn

doping in CuO film. It is clear from the literature survey that Mn doped CuO thin films were synthesized and characterized by several research groups for revealing different aspects of the material. No sufficient literature was found on the Mn doped CuO synthesized at relatively low substrate temperature with subsequent post deposition annealing. There are still a lot of scopes for widespread investigation on the structural, morphological, optical, and electrical properties of the material. The principal purpose of this research was to realize the applicability of Mn doped CuO as an absorber material for solar cells.

2. Materials and methods

2.1. Precursor Materials

The precursor salts used in this work were copper acetate monohydrates [$Cu(CH_3COO)_2.H_2O$] and manganese acetate [$Mn(CH_3COO)_2$] (purity 99%, MERCK, KGaA, 64271 Darmstadt, Germany). Ethanol and acetone of AR grade, Merck (~99.00% purity) and double distilled water were used during the deposition procedures.

2.2. Thin film preparation

Spray solution of molar concentration 0.10 M was prepared by dissolving $Cu(CH_3COO)_2.H_2O$ into double distilled water for the CuO thin film. For the synthesis of Mn doped CuO films with the Mn concentrations of 2, 4 and 6 at%, the ratio of $C_4H_6CuO_4.H_2O$ and $Mn(CH_3COO)_2$ in the spray solution was varied as per requirement. The precursor salts were stirred for 30 min using a magnetic stirrer and the mixture was filtered for ensuring the homogeneity. Few drops of ethanol were added to the spray solution to ensure better crystallization. The precleaned microscope glass substrate was placed in a substrate holder along with a mask of area 1.5×1.5 cm^2. A variac was used for adjustment of substrate temperature and a copper-constantan thermocouple was used for temperature measurement. The spray solution was sprayed onto the glass substrate at the constant substrate temperature of 523 K. The substrate to nozzle distance was kept fixed at 25 cm. The constant spray rate of 1.0 mL/min was maintained with the fixed compressor air pressure of 0.50 bar during the deposition process. Films were deposited for 10 min under the deposition conditions. Multiple beam interferometric (Fizeau fringe) method [25] was employed for measurement of film thickness. Film thicknesses were 182± 9.1, 181 ± 9.0, 168 ± 8.4 and 162 ± 8.1 nm for 0, 2, 4 and 6 at% Mn doped CuO thin films, respectively. The as-deposited CuO and Mn doped CuO thin films were annealed in air at the temperature of 723 K for 60 min in a Carbolite SHEFFIELD (England) tubular furnace.

2.3. Characterization of the films

X-Ray diffraction (XRD) analysis was carried out through an X-ray powder diffractometer [X'Pert PRO XRD Philips PW3040, Netherlands], operated with X-rays of

wavelength 1.5417 Å from CuKα target at input power of 60 kV and 55 mA. The 2θ values, d-spacing value, and full width at half maximum (FWHM) were studied using an "X'Pert Highscore" computer software. A scanning electron microscope [JEOL JSM-6490LA, Japan] was used for taking the field emission scanning electron microscopic (FESEM) images of the thin films at 30,000 magnifications. The average particle size of CuO and Mn doped CuO thin films were measured by ImageJ software using the FESEM pictures. Compositional analysis of the films was accomplished via a JEOL EX-37001 (Japan) electron dispersive spectrometer connected with the SEM arrangement. Optical transmittance (T%) and absorbance (A) of CuO and Mn doped thin films were studied at room temperature (300 K) using a UV-visible spectrophotometer [OPTIZEN POP QX UV/Vis, Republic of Korea] in the 200-1100 nm wavelength range. A four-point probe set up was used for measurement of electrical resistivity of the thin films at room temperature and in the range of temperature 303 - 423 K.

3. Results and discussion

3.1. Structural analysis

The XRD pattern of as-deposited CuO thin film shows poor crystalline nature [20]. The as-deposited Mn doped CuO thin films show amorphous nature in XRD analysis. After annealing the films in air at 723 K for 60 min, CuO film shows monoclinic structure with the peaks along ($\bar{1}11$), (111), ($\bar{2}02$), (202) and ($\bar{1}13$) crystallographic planes (Fig. 1). The positions of the peaks matched with the standard JCPDS data card no. 01-073-6023 [26]. All these peaks are found in the XRD pattern of 2 at% Mn doped CuO film. ($\bar{1}11$) and (111) are the preferential peaks in the XRD pattern of all the samples. Intensity of ($\bar{1}11$) and (111) peaks increase for 2 at% Mn doping. 4 and 6 at% Mn doped thin film shows poor crystallinity with two less intense ($\bar{1}11$) and (111) peaks. No peak related to Mn or Mn-based oxides is found in Fig. 1.
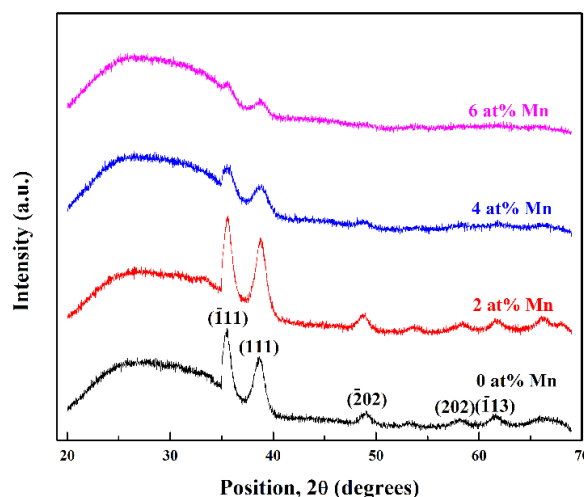

Fig. 1. XRD patterns of undoped and Mn *doped* CuO *thin films annealed in air at 723* K *for 60 min (color online)*

The nearly equivalent ionic radii of Cu^{2+} and Mn^{2+} encourage the creation of substitutional defects upon doping, without hampering the monoclinic structure of CuO. Crystallinity of CuO is better after 2 at% Mn doping which is evident by the improvement of peak intensities. For 4 and 6 at% Mn doping the samples is again less

crystalline. These diffraction patterns show that above 2 at% Mn doping in CuO caused the crystallinity to deteriorate whereas 2 at% Mn doping has a generative effect on crystallinity [9].

Table 1. Structural parameters of annealed Mn *doped* CuO
thin films for ($\bar{1}11$) *peak*

Mn conc. (at%)	2θ (deg)	d-spacing (nm)	D (nm)	ε × 10^{-3}	δ × 10^{-3} (nm^{-2})
0	35.57	0.2521	10	3.26	8.83
2	35.47	0.2528	11	3.10	8.01
4	35.51	0.2524	16	2.12	3.75
6	35.54	0.2526	19	1.82	2.78

Table 1 shows the structural parameters corresponding to the most predominant ($\bar{1}11$) peak. The position of ($\bar{1}11$) peak shifts to lower angle upon 2 at% Mn doping relative to CuO film. ($\bar{1}11$) peak position (2θ) is shifted to higher angle upon 4 and 6 at% Mn doping. d-spacing corresponding to ($\bar{1}11$) peak is found to be almost similar for all the films. It can be said that the monoclinic structure is unaltered but since there is a slight difference in ionic radii of Cu^{2+} and Mn^{2+}, the effect of substitution appears in the form of shift in ($\bar{1}11$) peak position.

Crystallite size (D) is calculated using the Scherrer formula (equation 1), where k is a constant called shape factor, λ is the X-rays wavelength, β is the FWHM and θ is the Bragg angle. Micro strain (ε) and dislocation density (δ) are computed using the following equations (2) and (3).

$$D = \frac{k\lambda}{\beta \cos\theta} \qquad (1) \; [27]$$

$$\varepsilon = \frac{\beta \cos\theta}{4} \qquad (2) \; [28]$$

$$\delta = \frac{1}{D^2} \qquad (3) \; [29]$$

Table 1 shows that D increases from 10 to 19 nm with increasing Mn doping in CuO. Gulen et al. [9] also observed larger D for increasing Mn concentration. In Table 1, it is observed that ε and δ decrease as D increased. These results agree well with the findings published in a paper on Mn doped CuO nanoparticles prepared by green synthesis [30].

3.2. Surface morphological analysis

FESEM pictures of annealed samples are shown in the Fig. 2.

In Fig. 2(a), the surface of the undoped CuO thin film is comprised of clusters of nanoparticles. The nanoparticles clusters are more clearly observed in Fig. 2(b - d) compared with Fig. 2(a). In Fig. 2(b), the nanoparticles are more evenly distributed in the surface of 2 at% Mn doped CuO film compared to other films. This is a clear consequence of improved crystalline structure of CuO for 2 at% Mn doping. The nanoparticles' clusters are found far from each other in Fig. 2(c). In Fig. 2(d), the nanoparticles' clusters join together to form larger agglomerates. As a consequence, 4 and 6 at% Mn doping cause no further improvement in crystallinity of the CuO films.
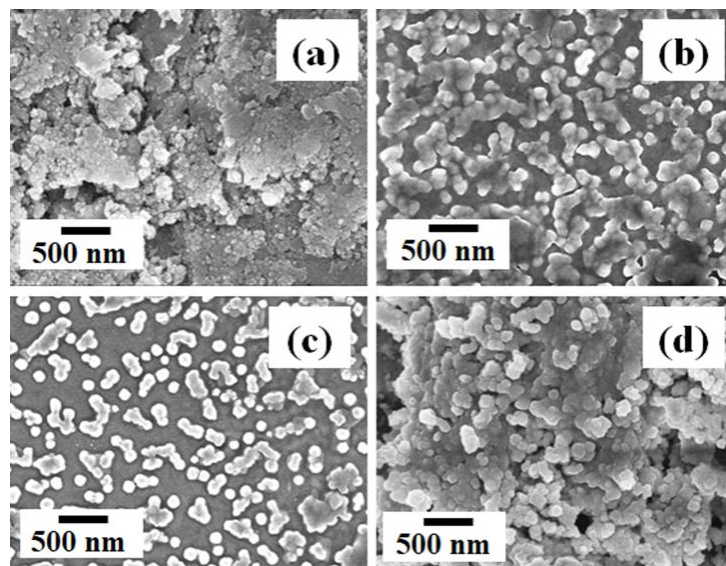

Fig. 2. FESEM pictures of (a) undoped, (b) 2, (c) 4 and (d) 6 at% Mn *doped* CuO *thin films annealed in air at 723* K *for 60 min*

The average particle sizes of 0, 2, 4 and 6 at% Mn doped CuO thin films are 11.91, 21.60, 23.09 and 24.93 nm, respectively. The increase of average particle size with increasing Mn concentration can be correlated with the elevation of crystallite size found in XRD analysis. The average particle size differs slightly with some earlier literatures [22, 23] because of differences in deposition parameters like precursor material, substrate temperature, etc.

3.3. Compositional analysis

The EDX spectra of annealed Mn doped CuO thin films with various Mn concentrations are shown in Fig. 3 and the data extracted from the spectra are displayed in Table 2.
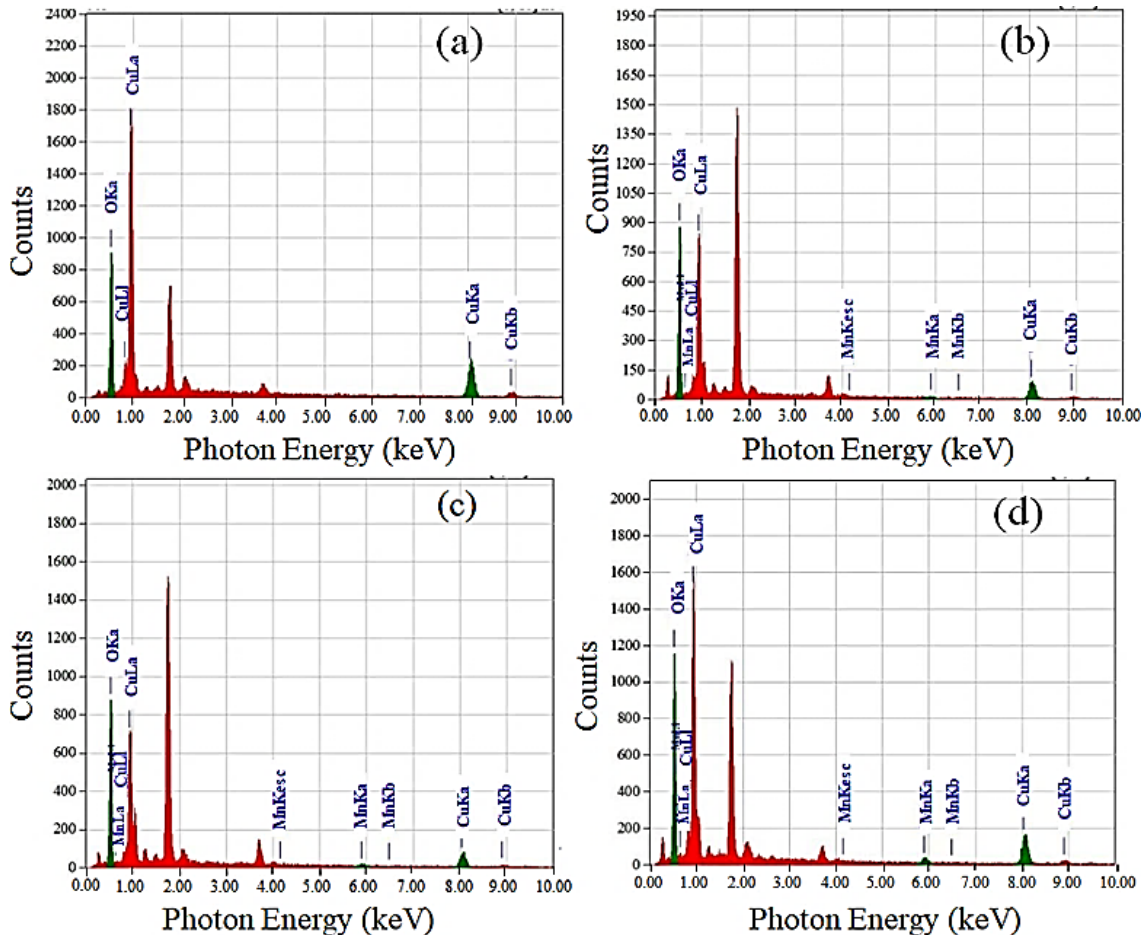

Fig. 3. EDX spectra of (a) undoped, (b) 2, (c) 4 and (d) 6 at% Mn doped CuO thin films annealed in air at 723 K for 60 min (color online)

Table 2. Data of compositional analysis of annealed CuO and Mn doped CuO thin films

Mn conc. (at%)	Element	Mass %	Atom %
0	O	15.32	41.81
	Cu	84.68	58.19
2	O	26.87	59.22
	Cu	70.91	39.36
	Mn	2.21	1.42
4	O	30.64	63.52
	Cu	66.18	34.55
	Mn	3.18	1.92
6	O	20.75	50.77
	Cu	74.99	46.19
	Mn	4.26	3.03

EDX spectra of CuO thin film confirm the existence of Cu and O in the film indicated with green peaks in Fig. 3 (a). Additional peaks related to Mn are seen in Fig. 3 (b-d). Table 2 shows that, all the samples are stoichiometric, and the amount of Mn increases in the film with the rise of the amount of Mn doping in CuO. Although EDX cannot estimate the exact amount of the elements, still increase of Mn content in the Table 2 can be considered as rough evidence of successful incorporation of Mn in the CuO during the film formation.

3.4. Optical properties

The transmission spectra of annealed Mn doped CuO films are represented in Fig. 4. The films are more transparent in the near infrared (NIR) region of light. Transmittance (T) elevates with the increase of Mn concentration up to 4 at%. The maximum T of about 96% is found for 4 at% Mn doping. The increase of T can be connected to existence evenly distributed nanoparticles with well-defined boundaries as seen in Fig. 2. In published literature [9], T was reported to be increasing with Mn incorporation in CuO film attaining the maximum value about 80% for 0.10 at% Mn doping. T-value falls for 6 at% of Mn doping in CuO which may be because of clustering of nanoparticles on the surface and relatively less well-defined boundaries observed in Fig. 2(d).
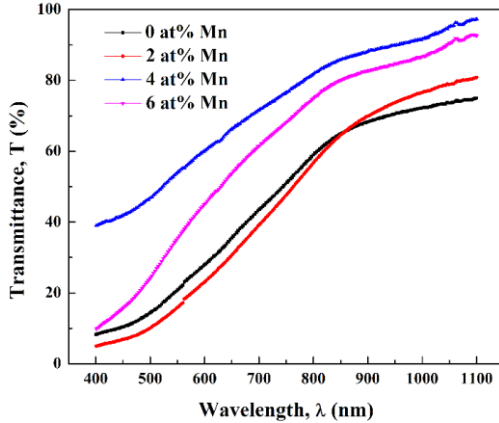

Fig. 4. Transmission spectra of Mn *doped* CuO *thin films annealed in air at 723* K *for 60 min (color online)*

According to the optical absorption theories, absorption coefficient (α) and photon energy (hν) are related as follows [31].

$$(\alpha h\nu) = B \ (h\nu - E_g)^{n'} \qquad (4)$$

In equation (4), E_g is the bandgap energy, B is a constant and the exponent n' depends on the nature of transition. For allowed direct transition $n'=1/2$ and for allowed indirect transition $n'=2$ [31]. α was calculated using the absorbance (A) data using the following equation [32].

$$\alpha = \frac{2.303 \ A}{d} \qquad (5)$$

where, 'd' is the film thickness. The optical band gap energy for the allowed direct transition was calculated using the plot of $(\alpha h\nu)^2$ versus hν which is known as the Tauc plot. Tauc plots of annealed undoped and Mn doped CuO thin films are shown in Fig. 5. The E_g-values estimated from the Tauc plot are exhibited in the Table 3. E_g increases in the range 2.09 to 2.45 eV with the increment of Mn doping. Incorporation of Mn^{2+} in CuO creates substitutional defects in the structure which influences the surface morphology and film composition as confirmed in FESEM and EDX analysis. E_g-values were reported between 2.00 and 1.91 eV for spray pyrolyzed Mn doped CuO thin films [33] and those was reported between 1.77 – 1.71 eV for Sol-gel prepared films [17]. The slight difference in E_g-values with the literature [33] and [17] happens because of differences in film preparation conditions and preparation technique, respectively.
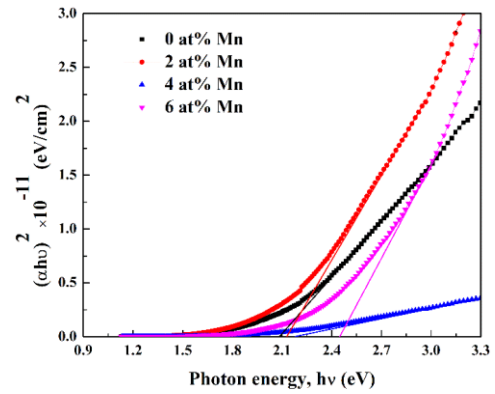

Fig. 5. Tauc plots of undoped and Mn *doped* CuO *thin films annealed in air at 723* K *for 60 min (color online)*

Extinction coefficient (k) of samples was calculated using α-values in the following relation [34].

$$k = \frac{\alpha\lambda}{4\pi} \qquad (6)$$

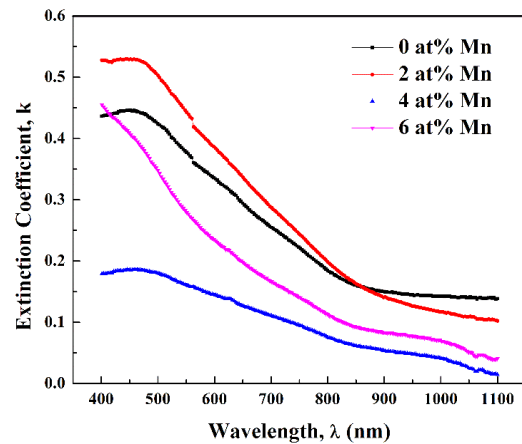*Fig. 6. Extinction coefficient of undoped and* Mn *doped* CuO *thin films annealed in air at 723* K *for 60 min (color online)*

Fig. 6 exhibits the variation of k-values with the photon wavelength. The 2 at% Mn doped CuO film shows the higher k-values in the visible light region compared to other films. It happens due to the creation of insufficient number Mn^{2+} substitutions in the CuO matrix for relatively lower doping. In the NIR region, the higher k-values are found for the undoped CuO film. k-values of CuO films are decreasing with the increase of Mn doping up to 4 at% in NIR region. It indicates the lessening of absorbing nature in NIR region of CuO occurs due to the homogeneous distribution of nanoparticles and sharp particle boundaries. The presence of agglomerated regions of nanoparticles causes the rise in k-values of 6 at% Mn doped CuO thin film in the vis-NIR. k-values of Mn doped CuO thin films stated in an earlier paper were in the range 0.2 to 0.8 [33]; which are in good agreement with those found in this work.

Refractive index (n) of samples was estimated using the following equation [35].

$$n = \left(\frac{1+R}{1-R}\right) + \sqrt{\left(\frac{4R}{(1-R)^2} - k^2\right)} \qquad (7)$$

In equation (7), reflectance (R) is calculated from T and A data.

The n-values of the thin films were also computed from the E_g-values using the Moss relation [32], Herve and Vandamme relation [36] and Ravindra and Gupta relation [37] given by equations (8), (9) and (10), respectively.

$$n(Moss) = \left(\frac{95}{E_g}\right)^{\frac{1}{4}} \text{ eV} \qquad (8)$$

$$n(HV) = \sqrt{1 + \left(\frac{A'}{E_g + B'}\right)^2} \qquad (9)$$

$$n(RG) = 4.084 - 0.62\,E_g \qquad (10)$$

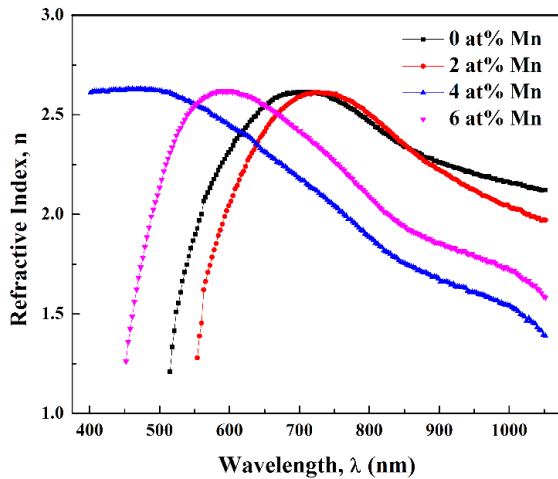In equation (9), A' is the hydrogen ionization energy ~13.6 eV and B' is 3.47 eV.

Fig. 7. Refractive index of undoped and Mn doped CuO thin films annealed in air at 723 K for 60 min (color online)

Table 3. Refractive indices of annealed CuO and Mn doped CuO thin films

Mn conc. (at%)	E_g (eV)	$n_{max}(vis)$	n(Moss)	n(HV)	n(RG)
0	2.09	2.62	2.60	2.64	2.79
2	2.13	2.61	2.58	2.65	2.76
4	2.19	2.61	2.56	2.66	2.72
6	2.45	2.63	2.49	2.71	2.56

Variation of n-values of annealed Mn doped CuO thin films are shown in Fig. 7. The n-values increase with wavelength reaching the maxima in the visible light region. n_{max} (vis)-values displayed in Table 3. n_{max} (vis)- values are almost independent of Mn doping. From Table 3, n(Moss) and n(RG) slightly decrease, and n(HV) remain almost constant with the increase of Mn doping from 0 to 4 at% in CuO thin films. The variation trend indicates that 2 and 4 at% Mn doped films allow light to pass more freely through and have less absorbing nature in the vis-NIR region. Here, n(Moss) and n(HV) are in good agreement with n_{max} (vis)-values, however n(RG) show slight overestimation for 0, 2 and 4 at% Mn doped samples. n(Moss) and n(RG) of 6 at% Mn doped film are the least, whereas n_{max} (vis) and n(HV) of this sample is the highest. In the Fig. 4 and Fig. 6, T-value drops, and k-value increases for 6 at% Mn doped film. So, logically the 6 at% Mn doped CuO film is more absorbing in nature and n(HV) is considered as more appropriate estimation for this sample than the others. The n-values match nicely with previously published literatures on CuO thin films [38, 39].

According to the Maxwell relation [34] shown in equation (11), the high frequency dielectric constants (ε_∞) of Mn doped CuO thin films were estimated using n(Moss), n(HV) and n(RG)-values.

$$\varepsilon_\infty = n^2 \qquad (11)$$

High frequency dielectric constant (ε_∞) and static (ε_o) were proposed by Adachi [40] as follows.

$$\varepsilon_\infty = 11.26 - 1.42\,E_g \qquad (12)$$

$$\varepsilon_o = 18.52 - 3.08\,E_g \qquad (13)$$

Table 4 shows that ε_∞ (Moss), ε_o, ε_∞ (RG), and ε_∞-values reduce, whereas ε_∞ (HV)-values rise with the increase of Mn doping in CuO films. Here, almost all dielectric constant values are showing decreasing trend with Mn doping. So, Mn doping have significant impact on ε_∞ and ε_o -values of CuO thin films. Thus, it can be said that Mn doping will help reducing the power loss in the CuO film and increase the suitability of the material for high frequency and power device applications [41].

For a compound semiconductor, the electron effective mass can be estimated using the following equation [42] and shown in Table 4.

Table 4. Dielectric constants and m_e^*/m_o of annealed CuO and Mn doped CuO thin films

Mn conc. (at%)	$\varepsilon_\infty(Moss)$	$\varepsilon_\infty(HV)$	$\varepsilon_\infty(RG)$	ε_o	ε_∞	m_e^*/m_o
0	6.74	7.01	7.77	12.08	8.29	0.18
2	6.68	7.05	7.64	11.96	8.23	0.19
4	6.59	7.11	7.43	11.77	8.15	0.20
6	6.23	7.37	6.58	10.97	7.78	0.22

$$\frac{m_e^*}{m_o} = 5.17004 - 7.46699\,E_g + 3.63286\,E_g^2 - 0.57525E_g^3 \quad (14)$$

The m_e^*/m_o-value increases with the increment of Mn concentration from 0 to 6 at% in CuO thin films. Increase of m_e^*/m_o-value indicates the possibility of reduction of electron mobility upon Mn doping. It is evident that m_e^*/m_o-value depend on E_g, n, ε_∞ and ε_o. It can be stated from the study of the dielectric parameters that Mn doping up to 6 at% Mn doped in CuO thin film significantly decreases the tendency of energy loss. But the 6 at% Mn doped CuO film has a slightly higher tendency to create obstacles to carrier movement due to a little higher m_e^*/m_o-value. The ε_∞, ε_o and m_e^*/m_o-values found in this work are in fair match with the previous literatures [38, 43].

3.5. Electrical properties

In Fig. 8, the variation of electrical resistivity (ρ) of annealed Mn doped CuO is exhibited as a function of Mn concentration. The order of ρ is found 10^3 Ω-m. In earlier literature, ρ was found in the order of 10^3 Ω-cm (i.e., 10^1 Ω-m) [11, 24] for Cd and Mn doping, correspondingly. The difference in order of ρ may occur because of the difference in type of dopants and deposition conditions. The ρ-value is observed to reduce with the elevation of Mn doping. It can be associated with change in structure, morphology and variation in the stoichiometric ratio due to the larger number of Cu ion vacancies and electrically neutral defects on the film surface [44].
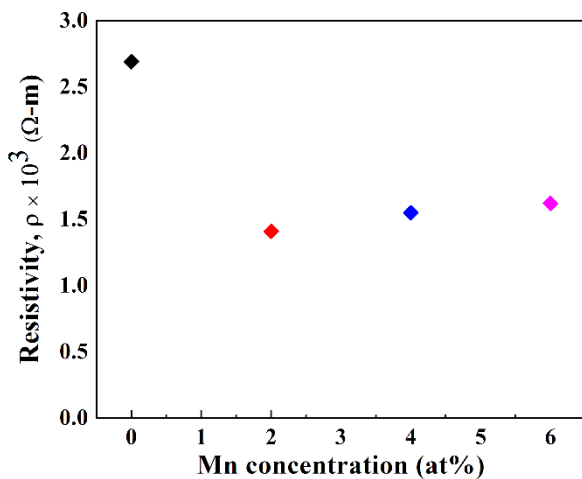

Fig. 8. Electrical resistivity versus Mn concentration plot of annealed CuO and Mn doped CuO thin films (color online)

The ρ-value of the thin films was measured in the temperature range from 303 to 423 K and the electrical conductivity (σ) was calculated. To determine the activation energy (ΔE) of the films, σ versus 1000/T graphs were drawn (Fig. 9). ΔE was evaluated using the following equation [45].

$$\sigma = \sigma_o exp\left(-\frac{\Delta E}{2k_B T}\right) \quad (15)$$

In equation (12), σ_o is the pre-exponential factor, k_B is the Boltzmann constant and T is the temperature in K.

Fig. 9 shows that σ of CuO and Mn doped CuO thin films increases non-linearly with temperature. So, there are two regions of electrical conduction with two ΔE-values for each sample. The ΔE-values are represented by ΔE_I in the temperature region 323 - 383 K and ΔE_{II} in the temperature region 383 - 423 K.
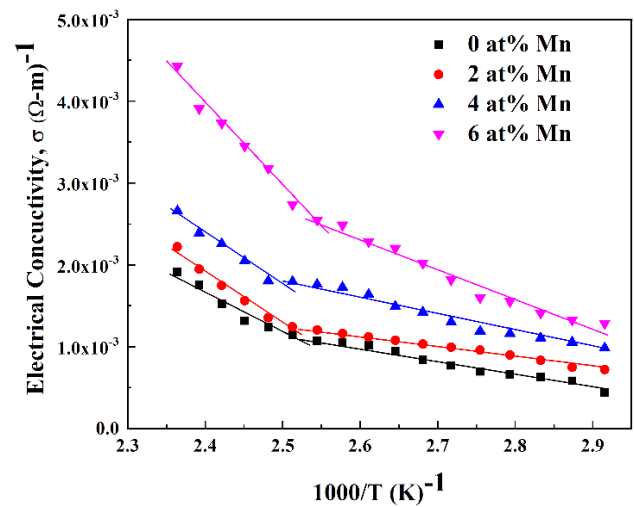

Fig. 9. Electrical conductivity versus 1000/T plots of CuO and Mn doped CuO thin films annealed in air at 723 K for 60 min (color online)

Table 5. Activation energies of annealed CuO *and* Mn *doped* CuO *thin films*

Mn conc. (at%)	ΔE_I (eV)	ΔE_{II} (eV)
0	0.29	0.39
2	0.14	0.32
4	0.08	0.29
6	0.13	0.40

Table 5 shows the variation of ΔE_I and ΔE_{II} with Mn doping in CuO thin films. ΔE_I is found between 0.08 and 0.29 eV and ΔE_{II} is found between 0.29 and 0.40 eV. Both ΔE_I and ΔE_{II} decrease with the elevation of Mn concentration up to 4 at% and then they increase for 6 at% Mn doping. Larger ΔE-values found for 6 at% Mn doped CuO thin film indicates the requirement of relatively higher energy for carrier hoping. It can be connected to the higher E_g, and m_e^*/m_o-values of the sample that makes the electron obstructed.

4. Conclusions

The effect of Mn doping on the structure and properties of CuO thin films deposited at 523 K are studied after annealing the films at 723 K in the air for 60 min. Monoclinic structure of the film is improved for 2 at% Mn doping, but it deteriorates for 4 and 6 at% Mn doping. Crystallite size increases with the increase of the amount of Mn doping in CuO thin films. Homogenously distributed nanoparticles with distinct boundaries are observed on the surface of 2 and 4 at% Mn doped CuO thin films. Particle size shows an increasing trend with the increase of Mn doping. Optical band gap is broadened upon the increase of Mn doping. CuO films shows more absorbing nature with relatively high extinction coefficient, refractive index, and dielectric constants for 2 at% Mn doping. Electron effective mass and electrical resistivity 2 at% Mn doped film is the least among all the doped samples. Activation energies in the temperature regions 323 - 383 K and 383 - 423 K decrease up to 4 at% Mn doping. Hence, 2 at% Mn doped CuO film has better crystalline structure, surface morphology, optical and electrical properties to be suitable for an absorber material in optoelectronic devices.

References

[1] D. Majumdar, S. Ghosh, J. Energy Storage **34**, 101995 (2021).
[2] H. Soonmin, E. Ajenifuja, Res. J. Chem. Environ. **23**(6), 138 (2019).
[3] M. Dahrul, H. Alatas, Irzaman, Procedia Environ. Sci. **33**, 661 (2016).
[4] S. Das, T. L. Alford, J. Appl. Phys. **113**, 244905 (2013).
[5] P. Sawicka-Chudy, M. Sibiński, E. Rybak-Wilusz, M. Cholewa, G. Wisz, R. Yavorskyi, AIP Adv. **10**, 010701 (2020).
[6] S. Baig, P. Kumar, J. Ngai, Y. Li, S. Ahmed, Chem. Phys. Chem. **21**(9), 895 (2020).
[7] J. M. Rzaij, N. F. Habubi, Appl. Phys. A **126**, 560 (2020).
[8] M. Nesa, M. Sharmin, K. S. Hossain, A. H. Bhuiyan, J. Mater. Sci.: Mater. Electron. **28**, 12523 (2017).
[9] Y. Gulen, F. Bayansal, B. Sahin, H. A. Çetinkara, H. S. Güderbet, Ceram. Int. **39**, 6475 (2013).
[10] F. Bayansal, T. Taskopru, B. Sahin, H. A. Cetinkara. Metall. Mater. Trans. A Phys. Metall. Mater. Sci. **45A**, 3670 (2014).
[11] M. H. Babu, J. Podder, B. C. Dev, M. Sharmin, Surf. Interfaces **19**, 100459 (2020).
[12] R. D. Shannon, Acta Crystallogr A **32**(5), 751 (1976).
[13] M. Iqbal, A. A. Thebo, A. H. Shah, A. Iqbal, K. H. Thebo, S. Phulpoto, M. A. Mohsin, Inorg. Chem. Commun. **76**, 71 (2017).
[14] K. P. Ganesan, N. Anandhan, G. Gopu, A. Amaliroselin, T. Marimuthu, R. Paneerselvam, J. Mater. Sci.: Mater. Electron. **30**, 19524 (2019).
[15] G. Durai, P. Kuppusami, K. Viswanathan, J. Mater. Sci.: Mater. Electron. **29**, 2051 (2018).
[16] L. Li, B. Lv, S. Wang, J. Z. Cai, W. Q. Zou, X. S. Wu, F. M. Zhang, J. Korean Phys. Soc. **62**, 1530 (2013).
[17] A. A. Manoharan, R. Chandramohan, R. D. Prabu, S. Valanarasu, V. Ganesh, M. Shkir, A. Kathalingam, S. AlFaify, J. Mol. Struct. **1171**, 388 (2018).
[18] A. H. Mustafa, M. M. Sadeer, S. A. Duha, Acta Phys. Pol. A **135**(4), 596 (2019).
[19] S. H. Narwade, V. V. Jadhav, R. S Mane, Solution Methods for Metal Oxide Nanostructures, Ch.9, Elsevier Science, London, 2023.
[20] P. Datta, M. Sharmin, J. Podder, S. Choudhury, J. Optoelectron. Adv. M. **23**(1-2), 35 (2021).
[21] H. Z. Asl, S. M. Rozati, Mater. Res. **21**(2), e20170754 (2018).
[22] H. A. Hussin, R. S. Al-Hasnawy, R. I. Jasim, N. F. Habubi, S. S. Chiad, J. Green Eng. **10**(9), 7018 (2020).
[23] M. J. Ismail, Z. T. Khodair, M. M. Kareem: Mater. Today: Proc. **49**(8), 3558 (2022).
[24] M. H. Babu, J. Podder: Mater. Sci. Semicond. Process **129**, 105798 (2021).
[25] S. Tolansky, Multiple Beam Interferometry of Surfaces and Films, Oxford Clarendon Press, London, 1948.

[26] F. C. Akkari, M. Kanzaria, B. Rezig, Eur. Phys. J. Appl. Phys. **40**(1), 49 (2007).

[27] P. Scherrer, N. G. W. Goettingen, Math-Phys. Kl **1918**, 98 (1918).

[28] Y. Zhao, J. Zhang, J. Appl. Cryst. **41**(6), 1095 (2008).

[29] G. K. Williamson, R. E. Smallman, Philos. Mag. **1**(1), 34 (1956).

[30] P. S. Vindhya, V. T. Kavitha, Chem. Pap. **77**, 2407 (2023).

[31] J. Tauc, Amorphous and Liquid Semiconductors, Springer, Boston, 1974.

[32] T. S. Moss, Photoconductivity in the Elements, Academic Press Inc., New York, 1952.

[33] K. A. Mishjil, K. Qader, W. A. Jabbar, Mater. Sci. **13**, 388 (2015).

[34] R. E. Hummel, Electronic Properties of Materials, 3rd ed., Springer-Verlag, New York, 2000.

[35] A. M. Alsaad, Q. M. Al-Bataineh, A. A. Ahmad, Z. Albataineh, A. Telfah, Optik **211**, 164641 (2020).

[36] P. J. L. Herve, L. K. J. Vandamme, Infrared Phys. Technol. **35**, 609 (1994).

[37] N. M. Ravindra, P. Ganapathy, J. Choi, Infrared Phys. Technol. **50**, 21 (2007).

[38] A. Moumen, B. Hartiti, P. Thevenin, M. Siadat, Opt. Quant. Electron. **49**, 70 (2017).

[39] V. Dhanasekaran, T. Mahalingam, J. Nanosci. Nanotechnol. **13**, 250 (2013).

[40] S. Adachi, Properties of Group IV, III–V and II–VI Semicondutors, Wiley, Chichester, 2005.

[41] E. A. Campo, Electrical Properties of Polymeric Materials: in Selection of Polymeric Materials, William Andrew Inc., New York, 2008.

[42] Y. Akaltun, Thin Solid Films **594**, 30 (2015).

[43] E. Güneri, J. Nano. Res. **58**, 49 (2019).

[44] S Baturay, A Tombak, D Kaya, Y. S. Ocak, M. Tokus, M. Aydemir, T. Kilicoglu, J. Sol-Gel Sci. Technol. **78**, 422 (2016).

[45] L. L. Kazmerski, Polycrystalline and Amorphous Thin Films and Devices, Academic Press, New York, 1980.

_____

*Corresponding author: jpodder59@gmail.com